Determination of Neutrino Oscillation Parameters and Simple Detector Effects

Keyi Liu

***Abstract*—This project aims to determine the neutrino oscillation parameters ϑ_{23} and Δm^2_{23} under two-flavour aapproximation and quantify the detector effects. Starting from an unoscillated prediction of the μ-neutrino energy spectrum, I apply the two-flavour survival probability to obtain an oscillated spectrum, which is then fitted to the binned event data using a Poisson negative log-likelihood. A simple parabolic minimiser is used first in 1-D and then extended to 2-D over (ϑ_{23} , Δm^2_{23}) with univariate method. I finally convolve the oscillated spectrum with a Gaussian detector response dominates by the central shift μ and the width σ, which are fitted simultaneously with the oscillation parameters. The best-fit values are $\theta_{23}/\pi = 0.2166^{+0.0060}_{-0.0054}$, $\Delta m^2_{23} = \left(2.423^{+0.035}_{-0.031}\right) \times 10^{-3}$ eV^2, $\mu = -0.090^{+0.016}_{-0.015}$ GeV and $\sigma = 0.097^{+0.021}_{-0.019}$ GeV.**

I. Introduction

NEUTRINOS are elementary particles in the Standard Model and appear as the neutral partners of the charged leptons e, μ and τ. They come in three flavours, ν_e, ν_μ and ν_τ. Neutrino oscillation is a quantum mechanical phenomenon that occurs if neutrinos have non-zero masses and the flavour eigenstates are mixtures of the mass eigenstates, so that a neutrino produced in one flavour can later be detected as another flavour [1]. Under two-flavour approximation, this oscillation is governed by the mixing angle θ_{23} and the mass-squared difference of the flavours Δm^2_{23}.

The aim of this project is to determine the best-fit values for these parameters by minimizing the Negative Log Likelihood (NLL). In addition, the analysis incorporates detector resolution to reflect realistic experimental conditions thus extracting more accurate oscillation parameters.

II. Theory

A. Survival probability of a muon neutrino

In two-flavour approximation where ν_μ and ν_τ mixing dominates, Eq. (1) gives the survival probability for a muon neutrino of energy E (GeV) after travelling a distance L (km), i.e. the probability that a ν_μ is still observed as ν_μ [1].

$$P(\nu_\mu \to \nu_\mu) = 1 - \sin^2(2\theta_{23})\sin^2\left(\frac{1.267\Delta m^2_{23} L}{E}\right) \quad (1)$$

Where θ_{23} is the mixing angle which determines the amplitude of the survival probability and Δm^2_{23} is the difference between the squared masses of the two neutrinos that influences the frequency of the oscillations and L is the travelling distance of a neutrino [1].

B. Poisson Negative Log Likelihood

In High Energy Physics experiments, the number of entries in each bin of a data histogram can be treated as a discrete measurement whose probability follows the Poisson distribution [1]. For a single bin with observed count m and expected mean λ, the probability is:

$$P(m) = \frac{\lambda^m e^{-\lambda}}{m!} \quad (2)$$

For many bins, the likelihood for the full spectrum ($\mathcal{L}$) is given by the product of the Poisson probabilities over all bins. Taking -2ln ($\mathcal{L}$) defines the Poisson negative log-likelihood (NLL) used in this project:

$$NLL(u) = 2\sum_{i=1}^{n} \lambda_i(u) - m_i \ln \lambda_i(u) + \ln m_i! \quad (3)$$

Here u denotes the set of parameters on which λ depends. The best-fit values of these parameters are obtained by minimizing NLL with respect to u.

III. Numerical Methods

A. Data

In this project, I first wrote a program to read the provided neutrino data file, which contains two columns of event counts binned in energy: the first column is the number of observed muon neutrino events, and the second column is the predicted event count from a Monte Carlo simulation under the "no oscillation" assumption. The energy range is 0–10 GeV and is divided into 200 equally spaced bins, so the bin width is $\Delta E = 0.05$ GeV. I defined the centre of the i-th bin as:

$$E_i = (i + 0.5)\Delta E \quad (4)$$

with $i = 0,1,\ldots,199$. Subsequently, I produced a histogram (Fig. 1) showing both the observed data and the non-oscillating prediction as functions of energy and visually compared their shapes to highlight the differences between the measured and predicted spectra.

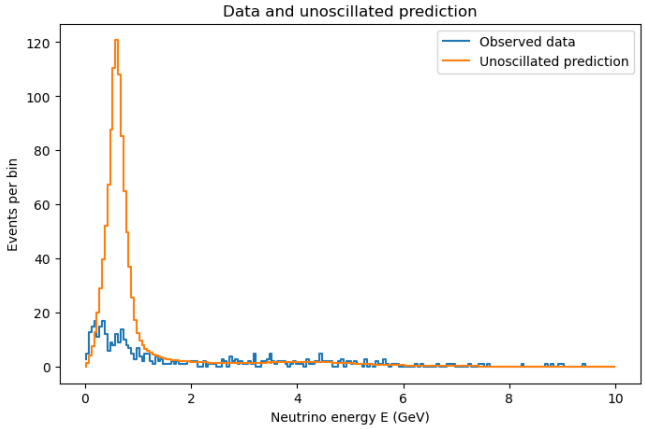

Fig.1: Histogram of the observed μ–neutrino events (blue) and the unoscillated prediction (orange) as a function of neutrino energy. Both spectra are shown in 200 equally spaced bins over the range 0–10 GeV.

B. The oscillated event rate prediction

Using Eq. (1) with a fixed baseline $L = 295$ km, I coded up the muon neutrino survival probability $P_{\mu\mu}(E; \vartheta_{23}, \Delta m^2_{23})$ and evaluated it for different choices of ϑ_{23} and Δm^2_{23}. The resulting curves, shown in Fig. 2(a) and 2(b), demonstrate that the survival probability at low energies is highly sensitive to these parameters, while it approaches unity at higher energies.

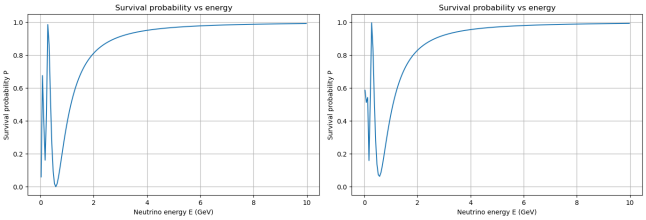

Fig. 2: μ–neutrino survival probability $P_{\mu\mu}(E)$ as a function of neutrino energy. Plot (a) (left) shows $P_{\mu\mu}(E)$ for the default parameter values $\vartheta_{23} = \pi/4$ and $\Delta m^2_{23} = 2.4 \times 10^{-3}$ eV^2, while plot (b) (right) shows the probability for $\vartheta_{23} = 0.21\pi$ and $\Delta m^2_{23} = 2.36 \times 10^{-3}$ eV^2.

To obtain the predicted oscillated event spectrum, I multiplied the unoscillated prediction N_i^{unosc} in each energy bin by the corresponding survival probability at the bin centre E_i:

$$\lambda_i(\vartheta_{23}, \Delta m^2_{23}) = N_i^{\text{unosc}}\, P_{\mu\mu}(E_i; \vartheta_{23}, \Delta m^2_{23}) \quad (5)$$

The resulting set of expected event counts $\{\lambda_i\}$ is plotted as shown in Fig. 3 and is used throughout the rest of the analysis as the fit function.

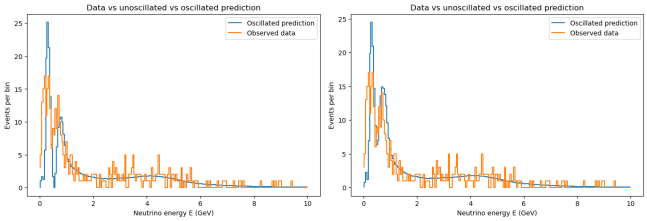

Fig. 3: Comparison of the observed μ–neutrino event spectrum (orange) with the oscillated prediction (blue) as a function of neutrino energy. Plot (a) (left) is generated using the default parameter values, while plot (b) (right) uses $\vartheta_{23} = 0.21\pi$ and $\Delta m^2_{23} = 2.36 \times 10^{-3}$ eV^2, which provide a visibly better description of the data and are therefore taken as a rough initial estimate of the oscillation parameters.

C. Negative Log Likelihood function

I implemented a function to compute the negative log likelihood (NLL) for each input parameter pair $(\vartheta_{23}, \Delta m^2_{23})$ to quantitatively compare the oscillated prediction with the observed data. The function calls the oscillated spectrum prediction algorithm to obtain the expected event counts λ_i in each energy bin and then sums over all

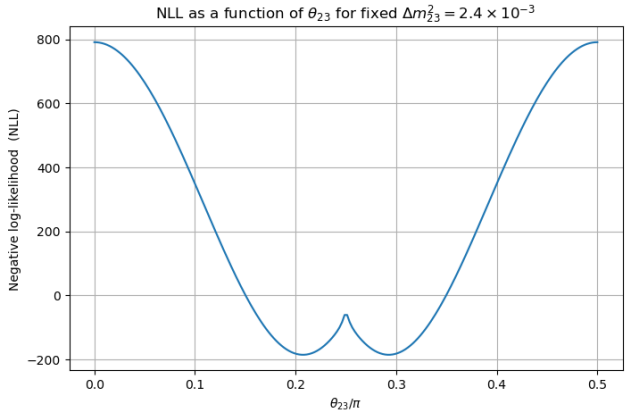

Fig. 4: NLL as a function of ϑ_{23}/π for a fixed value $\Delta m^2_{23} = 2.4 \times 10^{-3}$ eV^2. The curve exhibits two minima that are approximately symmetric about $\vartheta_{23}/\pi \simeq 0.25$, reflecting the octant degeneracy [2] which comes from $\sin^2(2\vartheta_{23})$. In the following analysis I focused on the lower-octant solution located near $\vartheta_{23} \approx 0.21\pi$, and treated it as the starting point for the one-dimensional minimizer.

bins according to Eq. (3) to return the corresponding NLL values. Since I am only interested in the location of the NLL minimum, constant terms that do not depend on the fit parameters are dropped to simplify the calculation. Fixing Δm^2_{23} to the default value 2.4×10^{-3} eV^2, I then evaluated NLL for a series of uniformly spaced ϑ_{23} values and plotted the resulting curve in Fig. 4 to locate the approximate position of the NLL minimum.

D. 1-Dimensional Minimizer

I found that the NLL(θ_{23}) curve is smooth and approximately parabolic near its minimum, and within the region $\theta_{23} \in [0.16\pi, 0.24\pi]$ there is only a single clear minimum. This behavior is suitable for using a parabolic minimizer. This method is simple to implement, requires no derivatives, and converges quickly in a single-minimum region where the function is close to quadratic. The algorithm uses three current points $\theta_1 < \theta_2 < \theta_3$ and their NLL values to fit a quadratic. Subsequently, it takes the vertex of this parabola as a new estimate θ_{new}, and updates the three points according to the position and value of θ_{new}. So, the middle point remains the current best value while the bracketed interval is progressively reduced. To validate the method, I first tested it on an analytic function:

$$f(x) = \sin x\,, \qquad x \in \left[\frac{\pi}{2}, \frac{3\pi}{2}\right] \tag{6}$$

which contain only a single global minimum at x=π. In this case, I used the initial points as x_1=π/2, x_2=3π/5 x_3=3π/2. The minimizer converged in 3 iterations to the analytic minimum, which could validate the method well. Then I applied the same algorithm to the experimental NLL(θ_{23}), choosing initial points $\theta_1 = 0.16\pi$, $\theta_2 = 0.21\pi$ and $\theta_3 = 0.24\pi$, with θ_2 close to the expected minimum. I set a convergence criterion that the change in the best θ_{23} between successive iterations should be smaller than 10^{-4} and the corresponding change in NLL be smaller than 0.01. And I also imposed a maximum of 100 iterations to avoid pathological behaviour. With Δm^2_{23} fixed to 2.4×10^{-3} eV^2, the algorithm converged within 5 iterations to a lower-octant solution $\theta_{23}/\pi \approx 0.2074$ with a minimum NLL of -186.18 as shown in Fig. 5. As can be seen from the figure, the minimum found by the parabolic minimizer lies at the bottom of the NLL valley, which can further validate its effectiveness in this analysis. Generally, this method is highly dependent on reasonable initial values and the condition that there is only one minimum value within the range. However, these issues can all be resolved in this project.

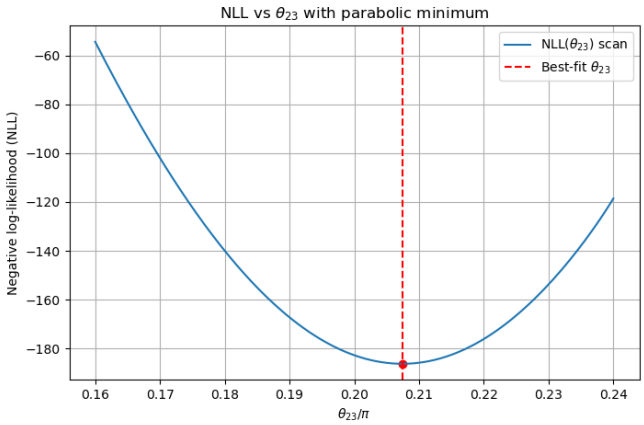

Fig. 5: Negative log likelihood as a function of θ_{23}/π for fixed Δm^2_{23}. The blue curve shows the one-dimensional scan of NLL(θ_{23}), while the red point and dashed line indicate the best-fit value obtained with the parabolic minimiser at $\theta_{23}/\pi \approx 0.2074$ (with $\text{NLL}_{\text{min}} \approx -186.18$).

E. Accuracy of the fit result

The values of θ^+_{23} and θ^-_{23} where the NLL is changed by 1.0 (in absolute units) compared to the value at the minimum correspond to a shift of one standard deviation in the positive and negative direction [1]. Using this property, I performed a scan of NLL(θ_{23}) with a range of 0.2 around the minimum and a step size of 1.0×10^{-5} along the θ_{23}/π axis to determine θ^+_{23} and θ^-_{23}. As shown in Fig. 6, these two points are symmetric about the minimum, yielding an uncertainty on θ_{23}/π of ± 0.0040.

To validate this result, I also estimated the uncertainty from the curvature of the final

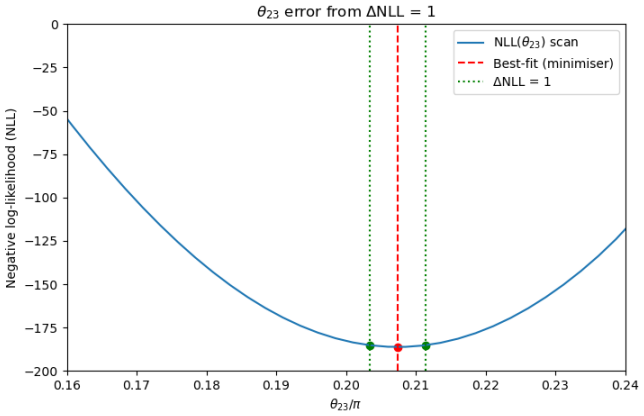

Fig .6: NLL as a function of θ_{23}/π around the minimum. The blue curve shows the one-dimensional scan of NLL(θ_{23}). The red point and dashed vertical line indicate the best-fit value of θ_{23} obtained from the parabolic minimiser. The green points mark the angles θ^-_{23} and θ^+_{23}, which are symmetric about the minimum, corresponding to an uncertainty on θ_{23}/π of ± 0.0040.

parabolic approximation to NLL(θ_{23})which can be written as:

$$NLL(\theta_{23}) = a\,\theta_{23}^2 + b\,\theta_{23} + c \qquad (7)$$

So that the error can be approximated by $\sigma_{\theta_{23}} \simeq 1/\sqrt{a}$ [3]. This gives $\sigma_{\theta_{23}} \approx \pm 0.0039$ which agrees with the ± 0.0040 obtained from the $\Delta\text{NLL} = 1$ method. Although the curvature method is more efficient computationally, it relies strongly on the assumption that the NLL is locally parabolic around the minimum, and its estimates can become unstable if the shape deviates from this ideal behaviour. I therefore adopt the uncertainty derived from the $\Delta\text{NLL} = 1$ method as the result to ensure robust error estimates.

F. 2-Dimensional Minimizer

To extract the two free parameters θ_{23} and Δm^2_{23} simultaneously, I performed a 2-D minimization to NLL and chose to use the univariate method. Compared with gradient or Newton's method, although univariate method converges more slowly and typically requires more iterations, it does not require analytic gradients or the Hessian matrix. Moreover, I have already validated and used the 1-D parabolic minimizer. Univariate method then became the most practical choice for this project.

I took the best-fit value of $\theta_{23}/\pi = 0.2074$ obtained in the one-dimensional scan and the default value of $\Delta m^2_{23} = 2.4 \times 10^{-3}\ \text{eV}^2$ as the starting point. In each iteration, I kept θ_{23} fixed and used the one-dimensional parabolic minimizer in the Δm^2_{23} direction to find the minimum of the NLL and then updated Δm^2_{23}. Since my 1-D minimizer requires 3 initial points, I took a small step $\Delta m = 2\times10^{-4}\ \text{eV}^2$ around the current estimation Δm^2_{23} thus obtaining the other two points used in the algorithm which were $\Delta m^2_{23} \pm \Delta m$. I fixed this updated Δm^2_{23} and repeated the 1-D minimization in the θ_{23} direction with $\Delta\theta = 0.2\pi$ subsequently. These two steps were alternated until they converged. In practice, I set the criteria for convergence that the change in NLL between consecutive iterations to be smaller than 0.01 and at which point the current values were taken as the best-fit parameters.

Before applying this algorithm to the real NLL, I validated it using a simple two-dimensional quadratic test function:

$$f(\theta, m) = (\theta - 0.6)^2 + (m - 0.003)^2 \qquad (8)$$

For which the global minimum at $(0.6\,,\,0.003)$ is known analytically. The minimizer converged to the test minimum within two iterations, confirming the correctness of the method. Then I Applied the algorithm to $\text{NLL}(\theta_{23}, \Delta m^2_{23})$, and it converged in four iterations to a minimum value $\text{NLL}_{\min} \approx -192.30$, with corresponding best-fit parameters:

$$\theta_{23}^{\text{best}} \approx 0.2082\,\pi;\ \Delta m_{23}^{\text{best}} \approx 2.360 \times 10^{-3}\ \text{eV}^2$$

The minimum NLL obtained with the 2D minimizer ($\text{NLL}_{\min} \approx -192.30$) is slightly smaller than the value obtained from the 1D scan with fixed Δm^2_{23} ($\text{NLL}_{\min} \approx -186.18$) as expected when releasing an additional degree of freedom. This means that 2D model gives a better fit and provides an additional consistency check of the univariate method I used.

Since θ_{23} and Δm^2_{23} are fitted simultaneously and are correlated, simply fixing one parameter and performing a one-dimensional uncertainty method would underestimate the true error. To mitigate the impact of nuisance parameters, I used the profile likelihood method [4].

In practice, I scanned a series of θ_{23} values around the 2-D best-fit point, with a scanning range 0.2π and a step size $\Delta\theta/\pi = 1.0 \times 10^{-4}$. For each of the fixed θ_{23}, I treated Δm^2_{23} as the only free parameter and applied the 1-D minimizer along the Δm^2_{23} direction to find the value that minimizes the NLL. The corresponding minimum was recorded as $\text{NLL}_{\text{prof}}(\theta_{23})$, which already accounts for the optimal choice of Δm^2_{23} at each θ_{23}. After scanning, I again used $\Delta\text{NLL} = 1$ method to the $\text{NLL}_{\text{prof}}(\theta_{23})$ 1-D profile curve and obtained the corresponding error on θ_{23}:

$$\theta_{23}/\pi = 0.2082^{+0.0040}_{-0.0040}$$

By repeating the same algorithm to Δm^2_{23} but swapping the nuisance parameter I got:

$$\Delta m^2_{23} = (2.423^{+0.050}_{-0.050}) \times 10^{-3}\ \text{eV}^2$$

The resulting best-fit values and uncertainties are very close to those obtained from the earlier 1-D scan with Δm^2_{23} fixed. This behavior is the same as expected because the fixed default value of Δm^2_{23} used in the 1-D scan already lies close to the global 2-D optimum. In addition, there is no obviously strong correlation between θ_{23} and Δm^2_{23} in this dataset. In such a situation, the more rigorous 2-D profile-likelihood treatment can only refine rather than largely alter the 1-D estimates.

G. Resolution of the detector

In the real experiment, the detector does not measure the neutrino energy perfectly. A given true particle energy could be measured as a range of possible "reconstructed" particle energies [1]. To quantify this effect in analysis, I convolved the true particle energy spectrum $\lambda_i^{true}(\vartheta_{23}, \Delta m^2_{23})$

obtained from prediction with a simplified detector model and got a reconstructed spectrum λ_i^{reco} which would be compared with the real data. The detector could be modelled as a Gaussian:

$$G(\Delta E;\mu,\sigma) = \frac{1}{\sqrt{2\pi}\sigma}\exp\left[-\frac{(\Delta E-\mu)^2}{2\sigma^2}\right] \quad (9)$$

Where μ is an overall shift of energy scale, σ is the effective energy resolution and ΔE is the difference in energy between a true bin and reconstructed bins. Both σ and μ are assumed to be constant over the energy range for simplicity. Under this assumption, all events in each true energy bin are redistributed among the reconstructed energy bins according to the same Gaussian in ΔE. And the probability for a single event to migrate from a true bin i to a reconstructed bin j only depends on the difference $E_j - E_i$ rather than on the absolute energies. Using this property, I built a response matrix $R_{ij}(\mu,\sigma)$ on the discrete energy grids to describe the probability. For each true bin i, I first computed unnormalized Gaussian weights for all reconstructed bins j:

$$r_{ij} = \exp\left[-\frac{(\Delta E-\mu)^2}{2\sigma^2}\right] \quad (10)$$

These weights are then normalized row by row to ensure that the sum of the probabilities for all possible reconstructed energy bins equals to 1 for a fixed true bin:

$$R_{ij}(\mu,\sigma) = \frac{r_{ij}}{\sum_j r_{ij}} \quad (11)$$

Therefore, the reconstructed spectrum can be calculated using convolution in discrete form:

$$\lambda_j^{reco}(\vartheta_{23},\Delta m_{23}^2,\sigma,\mu) = \sum_{i=1}^{n} R_{ij}(\mu,\sigma)\lambda_i^{true}(\vartheta_{23},\Delta m_{23}^2) \quad (12)$$

I created two plots to visualize the effect of detector parameters and to further validate the code as shown in Fig. 7.

Finally, I obtained the new NLL that depends on $\vartheta_{23},\Delta m_{23}^2,\sigma,\mu$ by substituting λ_i with λ_i^{reco} in Eq (3). To extract the best value of the parameters, I extended the 2-D minimizer to 4-D using the same univariate method. It started with the initial $\vartheta_{23},\Delta m_{23}^2$ equal to the best fit values obtained in previous 2-D minimization, $\sigma = 0.01GeV$ and $\mu = 0GeV$. The step Δ for ϑ_{23} and Δm_{23}^2 was the same as those in 2-D cases, while I chose Δ=0.005 for both σ and μ. Also, simple bounds were imposed on all four parameters to keep the scan in a physically reasonable region (e.g. ϑ_{23} within the allowed octant, $\Delta m_{23}^2 > 0$ and $\sigma > 0$). The

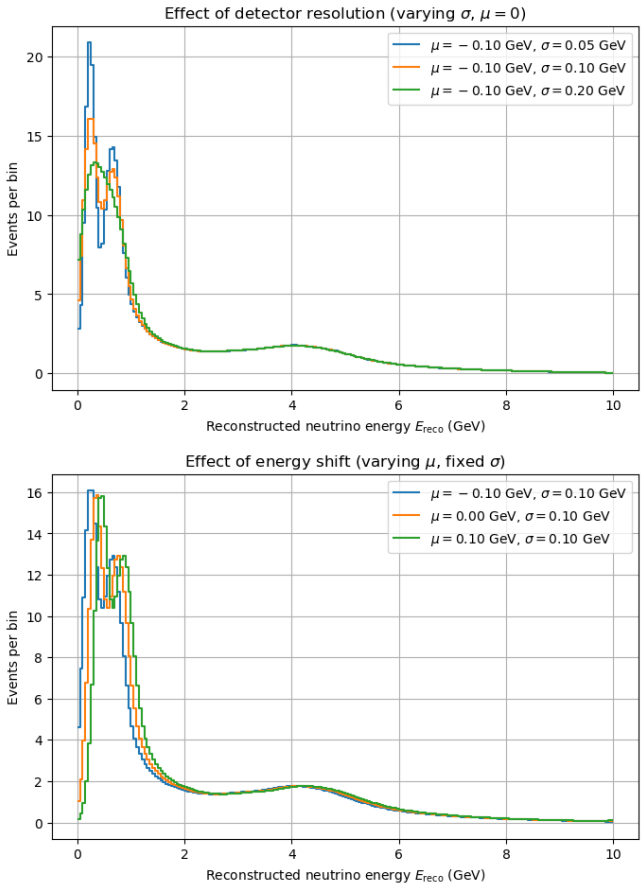

Fig. 7: (a) (top) The effect of detector resolution. Reconstructed spectra for different σ at fixed μ. As σ increases, the main peaks become lower and broader, and fine structures are smoothed out. (b) (bottom) Effect of an energy-scale shift. Reconstructed spectra for different μ at fixed σ. Changing μ shifts the main peak horizontally in energy.

iterations were stopped when the change in NLL between two successive iterations fell below 0.01.

To determine the uncertainties on the four parameters, I again used the profile likelihood method. When focusing on one parameter, the other three were treated as nuisance parameters and re-optimized using a three-dimensional extension of the univariate parabolic minimizer, yielding a profile NLL curve that depends only on the parameter of interest. The 1σ interval was then defined by the two points where the profile NLL increased by 1 with respect to its minimum.

IV. Results & Discussion

Considering the detector response in NLL leads to the following best fit parameter values:

$$\vartheta_{23}/\pi = 0.2166^{+0.0060}_{-0.0054};$$
$$\Delta m_{23}^2 = (2.423^{+0.035}_{-0.031}) \times 10^{-3}\ \text{eV}^2;$$
$$\mu = -0.090^{+0.016}_{-0.015}\ \text{GeV};\ \sigma = 0.097^{+0.021}_{-0.019}\ \text{GeV}$$

And NLL_{min} converged to -317.0 after 6 iterations. The reconstructed spectrum evaluated at this best fit point is shown in Fig. 8. The predicted spectrum

with the detector response closely matches the overall shape of the observed data. The position and amplitude of the low-energy peak as well as the high-energy decay trend are accurately reproduced. The minor residual fluctuations in the data are consistent with Poisson statistical variations.

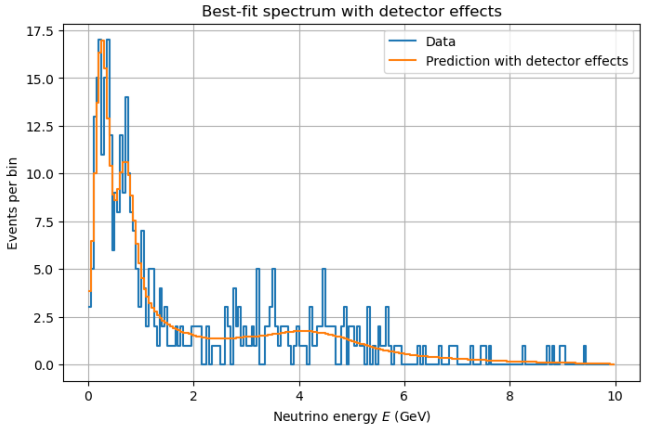

Fig. 8: Best-fit reconstructed spectrum with detector effects. Data (blue) and the prediction including Gaussian detector (orange) are generally matched.

The best-fit 4D values of ϑ_{23} and Δm^2_{23} are close to those obtained in the 2D fit, indicating that the oscillation pattern extracted from the data is robust against the introduction of the simplified detector model. The new parameters μ and σ provide a simple, physically interpretable description of the detector response: μ corresponds to a small overall underestimation of the reconstructed energy, while σ implies an effective energy resolution at the level of about 10–15% in the region around 1 GeV where most events are located. The difference between the minimum NLL values in the 2D and 4D fits is $\Delta\text{NLL} \approx -119$, which demonstrates a substantial improvement in the model once detector effects are included.

The obtained uncertainties are slightly asymmetric for all four parameters. This is because the profile NLL is not exactly a symmetric parabola around the minimum, and there are non-negligible correlations between the parameter of interest and the remaining ones, so the NLL generally rises at different rates when moving to lower or higher values of the parameter. In terms of scale, the relative uncertainties on ϑ_{23} and Δm^2_{23} are at the level of 2%-3% and about 1-2% respectively, indicating that the oscillation parameters are well constrained by the data. In contrast, the relative uncertainties on μ and σ are around 15–20%, reflecting the weaker constraints on the detector calibration and resolution in this simplified experimental configuration.

Overall, the asymmetric errors obtained from the profile likelihood are more conservative than those from the curvature method and provide a more realistic description of the impact of non-linearity and parameter correlations in the multi-parameter fit.

V. Conclusion

In this project I extracted the neutrino oscillation parameters ϑ_{23} and Δm^2_{23} by fitting a predicted oscillated spectrum to binned event data using a Poisson negative log likelihood. I first implemented a 1-D parabolic minimiser to locate the best-fit point in ϑ_{23} with its uncertainty for a fixed Δm^2_{23} and then extended this to a two-dimensional minimisation using the univariate method and profile likelihood. Finally, I included a simplified detector model in which the response is approximated by a Gaussian in energy with a central shift μ and width σ. The best-fit parameters with uncertainties are $\theta_{23}/\pi = 0.2166^{+0.0060}_{-0.0054}$; $\Delta m^2_{23} = (2.423^{+0.035}_{-0.031}) \times 10^{-3}\ \text{eV}^2$; $\mu = -0.090^{+0.016}_{-0.015}$ GeV and $\sigma = 0.097^{+0.021}_{-0.019}$ GeV.

The analysis is still limited by some simplifying assumptions: a two-flavour oscillation framework and a detector response modelled as an energy-independent Gaussian. The univariate method to minimize is also relatively simple compared with some other global optimisation techniques. Future improvements could therefore include a full three-flavour treatment or introduce a more realistic non-Gaussian detector. These extensions would allow a more precise and robust determination of the oscillation parameters.

References

[1] Mark Scot, James Owen, “Project 1: A log-likelihood fit for extracting neutrino oscillation parameters”, Computational Physics 2025-26, Imperial College London.

[2] S. K. Agarwalla, S. Prakash and S. Uma Sankar, “Resolving the octant of $\theta_{(23)}$ with T2K and NOvA,” *JHEP* **07**(2013) 131, arXiv:1301.2574 [hep-ph].

[3] R. A. Fisher, *On the mathematical foundations of theoretical statistics*, *Phil. Trans. R. Soc. Lond. A* **222**, 309–368 (1922).

[4] G. Cowan, K. Cranmer, E. Gross and O. Vitells, “Asymptotic formulae for likelihood-based tests of new physics,” *Eur. Phys. J. C* **71**, 1554 (2011), arXiv:1007.1727 [physics.data-an].